

CommonRoad-Game: A Human-in-the-Loop Simulation Framework for Autonomous Driving

Yunfei Bi and Youran Wang
Technical University of Munich
Munich, Germany
Email: {yunfei.bi, youran.wang}@tum.de

Abstract—Motion planning algorithms should be evaluated in human-in-the-loop environments to ensure they produce safe and efficient behaviors during interactions. However, existing simulation platforms often rely on recorded datasets, lack dedicated interfaces for real-time human interaction, or remain weakly integrated with an autonomous driving ecosystem. Moreover, many human-in-the-loop simulators are computationally intensive by design, making them less suitable for rapid prototyping and flexible experimentation in early-stage autonomous driving research. To address these limitations, we present **CommonRoad-Game**, a lightweight human-in-the-loop simulation framework tightly integrated with the CommonRoad platform, focusing on the systematic testing of motion planners with human participation and the analysis of human driving behaviors in interactive scenarios. We introduce a multi-threaded architecture with a robust synchronization mechanism that aligns simulation time with wall-clock time, enabling deterministic and temporally consistent interaction between autonomous and human-driven vehicles. In addition, the framework provides a scenario generation module that records driving logs, allowing diverse and reproducible test cases to be constructed from human-in-the-loop experiments. Experimental results demonstrate that **CommonRoad-Game** achieves stable temporal synchronization, supports scalable multi-agent simulation, and seamlessly integrates CommonRoad-compatible motion planners to generate interactive driving scenarios. The source code is publicly available at <https://github.com/Yunfei-Bi8/CommonRoad-Game>.

I. INTRODUCTION

Making safe and efficient decisions in interactive driving scenarios is a critical capability for motion planning algorithms in autonomous driving. Driving inherently involves complex interactions between autonomous vehicles (AVs) and human drivers, requiring the ability to understand and respond to human behavior. In situations such as merging, yielding, or navigating shared road spaces, where agents continuously adapt to each other’s actions, even minor variations in driving decisions may lead to substantially different outcomes [1]. Consequently, reliable experimental platforms for studying human driving behaviors and the interactions among human-driven vehicles (HVs) and AVs have become increasingly important. However, real-world experiments with physical vehicles are often costly, risky, and difficult to scale.

Fig. 1 summarizes the motivation and overall workflow of this work: real human inputs are used to create interactive and potentially critical driving behaviors, which are then recorded as structured driving logs for subsequent scenario generation and analysis.

To address these challenges, we present **CommonRoad-Game**, a lightweight human-in-the-loop simulation framework that enables interactive evaluation of motion planners within the CommonRoad [2]¹ ecosystem and facilitates the transition from offline benchmarking toward more realistic human-in-the-loop testing.

In the experimental evaluation, we demonstrate the applicability of the framework with two representative motion planning algorithms: an Intelligent Driver Model (IDM)-based motion planner² and a reactive sampling-based motion planner³. Both planners are available within the CommonRoad ecosystem.

A. Related Work

This section reviews representative simulation platforms for autonomous driving research, with a particular focus on simulation fidelity, human-in-the-loop capability, and support for motion planning evaluation.

High-fidelity, general-purpose simulators such as CARLA [3], LGSVL Simulator [4], and AirSim [5] provide realistic 3D environments with configurable sensors and physics. CARLA [3] is widely used for developing, training, and validating autonomous driving systems under diverse sensor suites and environmental conditions. LGSVL [4] emphasizes integration with full autonomy stacks such as Autoware⁴ and Apollo⁵, supporting both Software-in-the-Loop (SIL) and Hardware-in-the-Loop (HIL) testing. AirSim [5], built on Unreal Engine, supports both aerial and ground vehicles and enables software- and hardware-in-the-loop experiments via standard communication interfaces (e.g., MAVLink [6]).

Beyond high-fidelity simulators, MetaDrive [7] focuses on scalable scenario generation for reinforcement learning, enabling diverse traffic configurations via procedural composition and real-traffic data replay. Its design primarily targets large-scale data generation and policy training, rather than controlled interactive studies with human participants.

¹CommonRoad website: <https://commonroad.in.tum.de/>

²CommonRoad IDM planner: <https://gitlab.lrz.de/cps/commonroad/commonroad-idm-planner>

³Reactive planner: <https://gitlab.lrz.de/cps/reactive-planner>

⁴Autoware: Open-Source Software Stack for Autonomous Driving, <https://www.autoware.org/>

⁵Apollo: An Open Autonomous Driving Platform, <https://www.apollo.auto/>

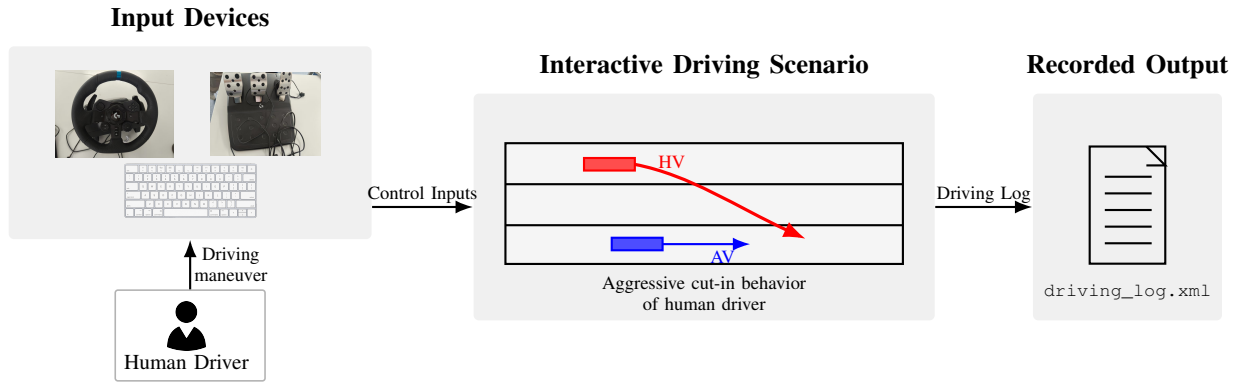


Fig. 1. Motivation and overall workflow of CommonRoad-Game. Human driver inputs are used to generate interactive driving behavior, including safety-critical maneuvers such as aggressive cut-ins between a human-driven vehicle (HV, red) and an autonomous vehicle (AV, blue). The resulting interaction is recorded as a structured driving log for scenario generation and analysis.

Closer to lightweight human-in-the-loop settings, CARLO [8]⁶ (*CARLA-Low Budget*) is a 2D simulator designed for HVs. It provides an interface to consumer-grade driving hardware, a simplified vehicle model for mapping real-time control inputs to trajectories, and a lightweight visualization environment. CARLO has proven effective for studying human driving behavior in controlled settings, particularly for reinforcement learning research.

Overall, existing simulation platforms reflect different design trade-offs. High-fidelity simulators prioritize visual realism, sensor modeling, and full-stack autonomy, often at the cost of increased system complexity and computational overhead. Lightweight simulators enable rapid prototyping and human-in-the-loop studies, yet typically provide limited support for structured motion planning evaluation under standardized benchmark formats. These observations motivate simulation frameworks that balance lightweight design with systematic support for interactive planner evaluation.

B. Contributions

Inspired by CARLO [8], we develop **CommonRoad-Game**, a lightweight human-in-the-loop simulation framework tightly integrated with the CommonRoad [2] ecosystem. Compared with CARLO, which focuses on HV simulation, and with general-purpose platforms such as MetaDrive [7], AirSim [5], LGSVL Simulator [4], and CARLA [3], CommonRoad-Game is designed for systematic interactive planner evaluation while remaining lightweight. The main contributions are summarized as follows:

- **Interactive Evaluation of Motion Planners:** We provide a standardized setup for assessing the safety and robustness of CommonRoad motion planners in scenarios involving real human participants.
- **Traffic Scenario Generation:** We support recording and replay of human driving logs, with direct export to the CommonRoad scenario format, enabling the collected interaction data to be reused for training data-driven

driving models as well as for systematic evaluation and benchmarking of motion planners.

- **Behavioral Capture and Analysis:** We provide high-fidelity logging of human driving behavior to support quantitative analysis of human–AV interactions.
- **Multi-Agent and Multi-Interface Simulation:** We support multi-AV scenarios and multiple human input interfaces (e.g., keyboard and steering wheels) for HVs, while maintaining temporal consistency between simulator execution and planner scenario time through a multi-threaded architecture.

II. PRELIMINARIES

A. CommonRoad

CommonRoad [2]⁷ is a benchmark framework and scenario format for motion planning of road vehicles. It aims to make motion-planning experiments reproducible and comparable by describing the relevant elements of a planning problem in a standardized form, including the road network, static and dynamic obstacles, vehicle models, planning goals, constraints, and cost functions. In this way, a benchmark can be specified by a compact identifier while still providing the information needed to reconstruct the corresponding planning problem.

In this work, CommonRoad [2] serves as the common representation layer between human-in-the-loop simulation and motion planner execution. HV states recorded in the simulator are mapped to CommonRoad-compatible dynamic obstacles, while planner outputs are interpreted as trajectories in the CommonRoad scenario frame. This standardized representation enables the proposed framework to reuse existing CommonRoad scenarios and planners, and to export recorded interactions as CommonRoad scenario files for offline analysis and benchmarking.

B. Curvilinear Coordinate Frame

Since our framework requires AVs and HVs to be tightly synchronized in one simulation frame (the global Cartesian

⁶CARLO repository: <https://github.com/Stanford-ILIAD/CARLO>

⁷CommonRoad website: <https://commonroad.in.tum.de/>

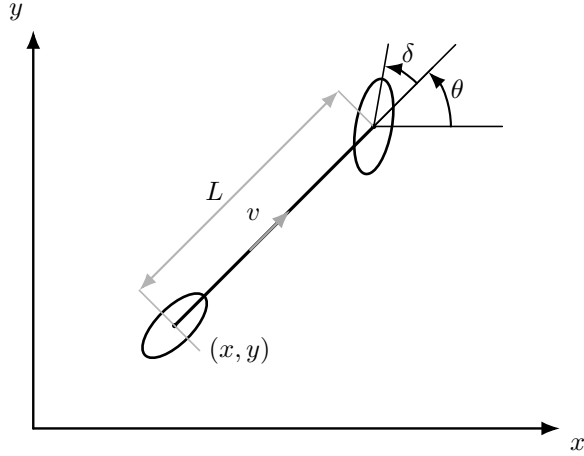


Fig. 2. Kinematic bicycle (single-track) model in the global Cartesian frame.

frame), while the motion planners sourced from CommonRoad [2] employed in this work usually perform planning in a curvilinear (Frenet) coordinate frame along a reference path, coordinate transformations between Cartesian and curvilinear coordinates are required. In our implementation, Frenet-coordinate conversion is performed using the robust curvilinear coordinate transformation toolbox of Würsching and Althoff [9].

A curvilinear coordinate frame is defined with respect to a given reference path Γ [9]. Instead of representing a planar position by Cartesian coordinates $\mathbf{p} = (x, y)^T$, the curvilinear representation uses (i) the arc-length s measured along Γ and (ii) the lateral (orthogonal) deviation d from the path point $\Gamma(s)$. Accordingly, a Cartesian point is mapped to curvilinear coordinates through a transformation

$$T_{\Gamma} : \mathbb{R}^2 \rightarrow \mathbb{R}^2, \quad (x, y) \mapsto (s, d). \quad (1)$$

C. Vehicle Model

In this work, we model the vehicle motion in the global Cartesian frame using the kinematic bicycle (single-track) model [2].

The state-space representation of kinematic bicycle model is given by

$$\dot{\mathbf{x}} = f(\mathbf{x}, \mathbf{u}), \quad (2)$$

where the state vector is

$$\mathbf{x} = [x, y, \theta, v, \delta]^T, \quad (3)$$

and the input vector is

$$\mathbf{u} = [a, \dot{\delta}]^T, \quad (4)$$

where the state variables are: $(x, y) \in \mathbb{R}^2$ denoting the rear-axle position in the global Cartesian frame, θ the heading angle, v the longitudinal velocity along the vehicle heading direction, and δ the front-wheel steering angle. The input variables are: a the longitudinal acceleration and $\dot{\delta}$ the steering rate. The parameter L denotes the wheelbase of the vehicle.

III. METHODOLOGY

We first include a drivability detection module that monitors the HV footprint for collisions and road-boundary violations using the CommonRoad [2] drivability checker package, then describe the remaining system components. The CommonRoad-Game simulation framework mainly consists of the following components:

- 1) a *CommonRoad Interface Module* that bridges the HV Simulator Module and motion planners by converting the simulation states of HVs into planner-compatible representations, and by mapping the resulting trajectories generated by motion planners back to the simulation domain. Through this state conversion and trajectory mapping process, the module ensures coordinate-frame and time synchronization between HV and AV behaviors,
- 2) a *Multi-threaded Simulation Architecture* that decouples the HV Simulator Module and Visualisation Module from the computationally intensive replanning process, enabling their execution in separate threads to ensure and analyze the synchronization between simulation time and real-world time,
- 3) an *HV Simulator Module* that acquires real-time control inputs from a Logitech G923 steering wheel and pedals⁸ and outputs the trajectory of HVs according to the control inputs,
- 4) a *Drivability Detection Module* that checks collision and road-compliance of the HV using the CommonRoad drivability-checker package⁹,
- 5) a *Visualisation Module* that translates CommonRoad scenarios into a customized visualization environment and visualizes the states of both AVs and HVs in a real-time manner,
- 6) a *Scenario Generation Module* that records the states of both AVs and HVs during simulations, converts these states into CommonRoad scenarios, and visualizes the scenarios in a frame-wise manner.

An overview of these components is illustrated in Fig. 3.

A. CommonRoad Interface Module

The CommonRoad Interface Module synchronizes HVs and AVs along two dimensions. First, it enforces *spatial synchronization* by establishing a fixed rigid-body transform between the simulator-side and the planner-side anchors of the global metric frame and applying it whenever states or trajectories are exchanged. Second, it enforces *temporal synchronization* by updating the HV and AV states in lockstep within each simulation cycle.

The following paragraphs detail these two aspects, respectively.

1) *Spatial Synchronization*: The simulator and the motion planner share the same global metric coordinate system defined by the CommonRoad [2] scenario, within which the HV

⁸Logitech G923 product page: <https://www.logitechg.com/de-de/shop/p/g923-trueforce-sim-racing-wheel>

⁹<https://commonroad.in.tum.de/tools/drivability-checker>

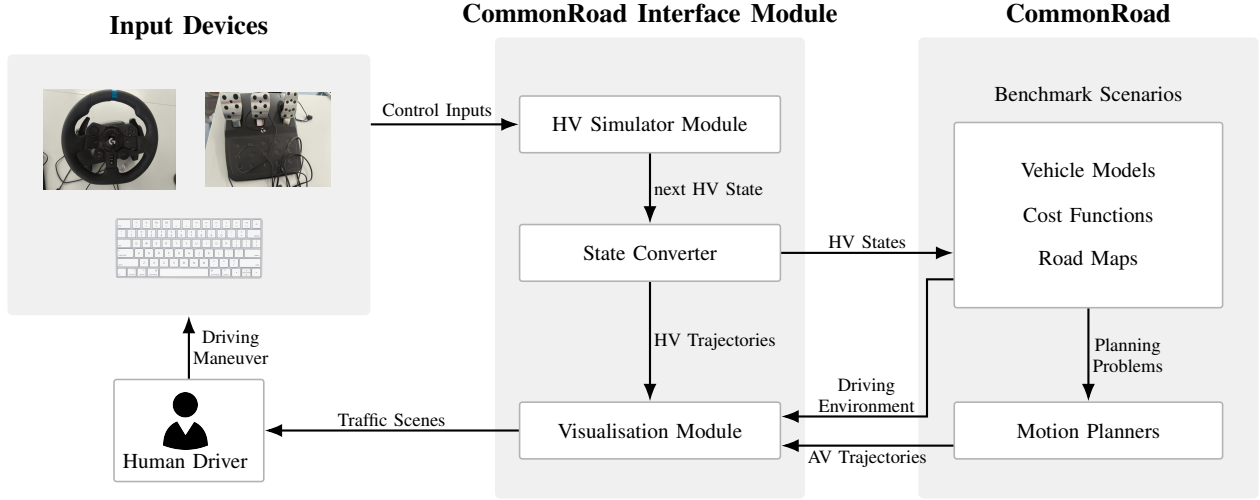


Fig. 3. Overview of the CommonRoad-Game simulation framework architecture.

and the AV are tracked and the planning problem is specified. At initialization, however, the simulator places the AV at a pose computed from the lanelet geometry, which is in general not identical to the initial AV pose declared in the planning problem. Spatial synchronization compensates for this initial-pose discrepancy through a fixed rigid-body transformation and two dedicated submodules that consistently map states and trajectories between the simulator-side and planner-side references throughout the simulation. For brevity, these two references are subsequently denoted as the *simulation coordinate system* and the *scenario coordinate system*, respectively; both correspond to the same underlying CommonRoad metric frame, but are anchored at the simulator-side and the planning-problem-declared initial AV poses.

a) Low-Level Simulation Module: The Low-Level Simulation Module advances the states of the HV and the AV at every simulation step by numerically integrating the kinematic bicycle model. Given the road network and initial vehicle poses provided by a CommonRoad [2] scenario, the module receives the driver's real-time control inputs (steering and acceleration/brake) and the trajectory states produced by the motion planner, and outputs the updated HV state x_h^{sim} and AV state x_a^{sim} at each simulation step. Both states are expressed in a shared simulation coordinate system:

$$\begin{aligned} x_h^{\text{sim}} &= [x_h, y_h, \delta_h, v_h, \psi_h]^\top, \\ x_a^{\text{sim}} &= [x_a, y_a, \delta_a, v_a, \psi_a]^\top. \end{aligned} \quad (5)$$

b) Frame-Alignment Module: To absorb the initial-pose discrepancy between the simulation and scenario coordinate systems, the Frame-Alignment Module estimates a rigid-body transform $T_{s \rightarrow c} = (R, \mathbf{d}, \Delta\psi)$ from the simulation coordinate system (s) to the scenario coordinate system (c), together with its inverse $T_{c \rightarrow s}$. The transform is computed once at initialization, held fixed throughout the simulation, and used to consistently map poses between the two references.

Denote the simulator-side and scenario-side initial AV poses

by (p_a^0, ψ_a^0) and $(\bar{p}_a^0, \bar{\psi}_a^0)$, respectively, where $p_a^0, \bar{p}_a^0 \in \mathbb{R}^2$ are planar positions, $\psi_a^0, \bar{\psi}_a^0$ are yaw angles, and the superscript 0 indicates the initial time step. Let $\text{wrap}_\pi(\cdot)$ denote the operator that normalizes an angle to $(-\pi, \pi]$, ensuring angular consistency and avoiding discontinuities at $\pm\pi$.

The module computes the yaw offset

$$\Delta\psi = \text{wrap}_\pi(\bar{\psi}_a^0 - \psi_a^0), \quad (6)$$

the rotation matrix

$$R = \begin{bmatrix} \cos \Delta\psi & -\sin \Delta\psi \\ \sin \Delta\psi & \cos \Delta\psi \end{bmatrix}, \quad (7)$$

and the translation vector

$$\mathbf{d} = \bar{p}_a^0 - R p_a^0. \quad (8)$$

For any pose $(p^{\text{sim}}, \psi^{\text{sim}})$ in the simulation coordinate system, the corresponding pose $(p^{\text{sc}}, \psi^{\text{sc}})$ in the scenario coordinate system is given by

$$\begin{aligned} p^{\text{sc}} &= R p^{\text{sim}} + \mathbf{d}, \\ \psi^{\text{sc}} &= \text{wrap}_\pi(\psi^{\text{sim}} + \Delta\psi), \end{aligned} \quad (9)$$

and conversely

$$\begin{aligned} p^{\text{sim}} &= R^\top (p^{\text{sc}} - \mathbf{d}), \\ \psi^{\text{sim}} &= \text{wrap}_\pi(\psi^{\text{sc}} - \Delta\psi). \end{aligned} \quad (10)$$

c) Human-Vehicle Scenario Adapter: The HV is presented to the planner as a dynamic obstacle through an adapter module. The adapter takes as input the current human state x_h^{sim} in the simulation coordinate system, the rigid transform $T_{s \rightarrow c}$ between the simulation and scenario coordinate systems, the current discrete scenario time index k , the simulation step size Δt , and a prediction horizon H_{pred} . It produces a dynamic obstacle in the scenario coordinate system whose current state matches the simulated HV at time index k , together with a short-horizon predicted trajectory of the same obstacle.

The adapter maps the simulated pose of the HV from the simulation coordinate system to the scenario coordinate system

using $T_{s \rightarrow c}$, and updates the corresponding dynamic obstacle state at time step k with the resulting position, yaw angle, and velocity. It then generates a short-horizon prediction over H_{pred} by forward propagating a constant-velocity, constant-steering kinematic model, expressed entirely in the scenario coordinate system. This provides the planner with a temporally and spatially consistent representation of the HV as a dynamic obstacle.

d) Autonomous Vehicle Interface: Distinct from the Frame-Alignment Module, which computes the transform $T_{s \rightarrow c}$ once at initialization, this module *applies* the (now fixed) transform bidirectionally at runtime. At every replanning trigger (Algorithm 1, lines 8–10), the current AV state x_{AV} is mapped to the scenario frame via $T_{s \rightarrow c}$ and packaged— together with velocity, yaw, acceleration, steering angle, yaw rate, and the scenario time index k —into the planner’s expected initial-condition format $x_{\text{AV}}^{\text{CR}}$. At every simulation step (Algorithm 1, line 13), the state $\tau[\lfloor \sigma \rfloor]$ retrieved from the current planner trajectory is mapped back via $T_{c \rightarrow s}$ and overwrites the AV simulation state. Because planner conventions differ (the reactive planner expects rear-axle positions, whereas the IDM planner uses center positions), the position is conditionally shifted between the rear axle and the vehicle center using the known wheelbase in the corresponding direction.

2) Time Synchronization: The framework involves two distinct time discretizations that, without explicit coordination, would drift apart and produce inconsistent state updates. The simulator advances at a nominal step Δt used to integrate the HV and AV dynamics, while the motion planner and the CommonRoad [2] scenario both operate on a coarser scenario time grid with step Δt_c that determines the temporal spacing of dynamic obstacle trajectories, predictions, and the planner’s trajectory states. The two steps are in general unequal: Δt is chosen by the simulator to be fine-grained so as to maintain real-time responsiveness to human input, whereas Δt_c is fixed by the scenario description and reflects the logical resolution at which the scenario evolves. Furthermore, the wall-clock cost of each simulation step is itself variable due to rendering, drivability checks, and I/O overhead, and the replanning routine is computationally expensive with non-constant runtime.

If left uncoordinated, these two cadences induce three concrete failure modes. First, the simulator’s wall-clock cadence diverges from Δt because per-step computation and replanning routinely stall the main loop, breaking the real-time responsiveness required for human-in-the-loop interaction. Second, the AV’s executed motion drifts off the planner’s intended trajectory because the trajectory is sampled at incorrect progress indices when Δt does not match Δt_c . Third, replanning requests fall on simulation steps that do not align with scenario-time boundaries, so the planner is re-initialized at a state inconsistent with the scenario’s discrete time grid.

To prevent these drifts, temporal synchronization updates HV and AV states in lockstep on a shared simulation timeline, while the planner maintains its internal scenario time indexing. This synchronization is realized through a set of submodules that coordinate state updates across the simulation timeline

Algorithm 1 Synchronization of HV and AV Timeline

Require: $\Delta t, \Delta t_c, T_{s \rightarrow c}, k_0$
1: $N \leftarrow \max(1, \text{round}(\Delta t_c / \Delta t))$
2: $n \leftarrow 0, k \leftarrow k_0, \sigma \leftarrow 0, \text{stop} \leftarrow \text{false}, \Delta t_{\text{wc}} \leftarrow \Delta t, t_0 \leftarrow \text{wall-clock}$
3: **while** $\neg \text{stop}$ **do**
4: **if** new planner result τ_{new} available **then**
5: $\tau \leftarrow \tau_{\text{new}}, \sigma \leftarrow \arg \min_i \|T_{c \rightarrow s}(\tau[i]) - x_{\text{AV}}\|$
6: **end if**
7: $u_h \leftarrow \text{READINPUT}(), x_h \leftarrow \Phi_{\text{KS}}(x_h, u_h, \Delta t_{\text{wc}})$
8: **if** $n \bmod N = 0$ **then**
9: $o_h(k) \leftarrow T_{s \rightarrow c}(x_h)$
10: $x_{\text{AV}}^{\text{CR}} \leftarrow T_{s \rightarrow c}(x_{\text{AV}}), \text{ENQUEUE REPLAN}(x_{\text{AV}}^{\text{CR}}, k)$
11: $k \leftarrow k + 1$
12: **end if**
13: $x_{\text{AV}} \leftarrow T_{c \rightarrow s}(\tau[\lfloor \sigma \rfloor])$
14: $\sigma \leftarrow \sigma + \Delta t / \Delta t_c$
15: **if** $\text{COLLISION}(x_h) \vee \text{OFFROAD}(x_h) \vee \text{USERSTOP}$ **then**
16: $\text{stop} \leftarrow \text{true}$
17: **end if**
18: $\text{WAITUNTIL}(t_0 + (n + 1)\Delta t), \Delta t_{\text{wc}} \leftarrow \text{measured interval}, n \leftarrow n + 1$
19: **end while**

and the planner’s scenario time base. Algorithm 1 presents a high-level pseudocode description of the time-synchronization procedure executed in each simulation cycle. Complementary, Fig. 4 visualizes the aligned HV/AV updates and the corresponding scenario-step boundaries within one simulation loop.

Notation. The framework involves *two distinct time discretizations*, both expressed in seconds. Their relationships are visualized in Fig. 4, whose three horizontal rows correspond to the HV update cadence, the AV update cadence, and the discrete scenario timeline, respectively.

(i) *Nominal simulation step* Δt is the simulator’s target tick interval at which the HV and AV states are advanced, indexed by the integer simulation step index n . It is a design choice of the simulator and is set fine-grained (typically 10 ms in our implementation) to maintain real-time responsiveness to human input.

(ii) *Scenario step* Δt_c is a scalar constant denoting the time interval (in seconds) between two consecutive points on the scenario timeline. It is declared by the CommonRoad [2] scenario file, is used to represent time-varying scenario elements (dynamic obstacle trajectories, predictions, and signal states), and is in general coarser than Δt (typically 100 ms in our implementation). The motion planner adopts the same step: its output trajectory is a sequence of states sampled at intervals of Δt_c .

The associated *scenario time index* k , distinct from Δt_c , is a dimensionless integer counter identifying the current position along this scenario timeline, related to Δt_c through the identity that scenario time equals $k \Delta t_c$ seconds. The index is initialized at k_0 (declared by the planning problem) and is incremented by one every $N = \text{round}(\Delta t_c / \Delta t)$ simulation steps, i.e., once per scenario interval; Fig. 4 illustrates the case $N = 3$, where the filled squares mark consecutive indices k and $k + 1$ and their spacing on the timeline equals Δt_c . The continuous progress variable σ further tracks the AV’s sub-step sampling position along the planner trajectory between

two consecutive scenario indices.

The two steps are unequal because they are fixed by different components: Δt is chosen by the simulator for fine HV/AV control granularity, whereas Δt_c is chosen by the CommonRoad scenario for logical-time resolution of the scenario and the planner. The time-synchronization mechanism aligns these two grids at scenario boundaries while keeping the per-step HV/AV update fine-grained.

The nominal step Δt is to be distinguished from the *realized* wall-clock interval Δt_{wc} , which is the actual elapsed real time between two consecutive cycles as measured by the global time-controller. Since no measured interval is yet available at the first cycle, Δt_{wc} is initialized to the nominal step Δt (Algorithm 1, line 2). Under the real-time invariant maintained by the framework, $\Delta t_{wc} \approx \Delta t$, but the two may transiently diverge under heavy computational load.

The remaining symbols are: u_h and x_h denote the human control input and the HV simulation state, respectively; x_{AV} is the AV simulation state, and x_{AV}^{CR} is its mapped state in the scenario coordinate system via $T_{s \rightarrow c}$. The planner trajectory is denoted by τ , a discrete sequence of states whose i -th element is written as $\tau[i]$, and the function $\Phi_{KS}(x, u, \Delta t)$ denotes the one-step propagation of the kinematic single-track model from state x under control input u over the duration Δt . The HV dynamic-obstacle representation written into the scenario at index k is denoted by $o_h(k)$, and t_0 is the wall-clock time recorded at simulation start. The stop flag is raised either by user termination or by drivability violations (collision or off-road).

We now describe the individual submodules that together realize the proposed time-synchronization mechanism.

a) *Global Time-Controller Module*: This module enforces the real-time invariant that the simulation’s virtual clock—a discrete counter advancing by Δt per control cycle—ticks at the same rate as the continuous wall-clock time reported by the operating system. Without enforcement, the per-cycle compute load would let the two timelines drift apart; the controller absorbs this drift by anchoring every cycle to a scheduled wall-clock deadline. The corresponding operations are highlighted in Algorithm 1.

This invariant is non-trivial to maintain because the per-cycle compute load is inherently variable. The motion planner, for instance, can take substantially longer than Δt to produce a new trajectory under heavy traffic or short scenario-time intervals, in which case it would fail to deliver a fresh trajectory in time for the next replanning boundary; even when its execution is decoupled onto a worker thread (Section III-B1), the main loop still incurs per-step costs for rendering, drivability checking, and the I/O acquisition of human control inputs, all of which are non-constant and can transiently exceed the step budget. Left uncompensated, these fluctuations would (i) let the virtual clock fall behind wall-clock time, breaking the real-time responsiveness required for HITL interaction with the human driver, and (ii) cause the HV dynamics to be integrated over the nominal Δt rather than the actual elapsed interval, leading to physically inconsistent

motion. The controller therefore needs to both pace the main loop against a wall-clock schedule and report the realized step duration to downstream consumers.

At simulation start, the controller records the wall-clock anchor t_0 (Algorithm 1, line 2). Each subsequent simulation cycle n is then assigned an *ideal* (scheduled) wall-clock start time

$$\tau_n^* = t_0 + n \Delta t, \quad (11)$$

i.e., the wall-clock instant at which cycle n is *supposed* to begin. Let τ_n denote the corresponding *actual* wall-clock time at which cycle n does begin. At the end of every cycle, the controller blocks the main loop in WAITUNTIL(τ_{n+1}^*) until the scheduled deadline of cycle $n+1$ is reached (Algorithm 1, line 18); upon resuming, it measures the actual elapsed wall-clock interval since the start of the just-finished cycle, $\Delta t_{wc} = \tau_{n+1} - \tau_n$, exposes the result downstream, and increments n . Fig. 5 illustrates the resulting alignment between the ideal τ_n^* , the realized τ_n , and the uniform simulation steps $n\Delta t$.

To quantify the deviation between realized execution and the ideal schedule, the controller tracks the per-step timing error and its accumulation,

$$\begin{aligned} e_n &= \Delta t_{wc} - \Delta t, \\ E_n &= \sum_{i=1}^n e_i, \end{aligned} \quad (12)$$

and exposes both quantities together with the per-cycle sleep duration for upstream monitoring. Three complementary mechanisms then maintain the alignment under variable computational load:

- 1) **Wall-clock pacing.** The blocking wait described above enforces $\tau_n \geq \tau_n^*$ whenever computation completes early. If the per-cycle computation exceeds the available budget, the wait reduces to zero and the simulation temporarily lags behind the ideal schedule.
- 2) **Adaptive frame skipping.** When the synchronization lag exceeds a tolerance threshold, the rendering pipeline is temporarily suppressed; bypassing visualization significantly reduces per-step compute, allowing the loop to run faster than real time and gradually amortize the accumulated drift *without* modifying the reference time.
- 3) **Drift reset.** As a last-resort fallback, the controller re-anchors the reference time t_0 to the current wall-clock and resets E_n whenever $|E_n|$ exceeds a preset threshold, preventing unbounded long-term drift. The reset is suppressed during a brief warm-up window at the start of simulation (the first few simulation steps) so that one-off startup transients—first-frame rendering, scenario loading, JIT compilation—do not artificially inflate E_n and trigger spurious resets.

Downstream, the controller clips the measured Δt_{wc} to a configured range $[\Delta t_{\min}, \Delta t_{\max}]$ to obtain the time step that is actually used to numerically integrate the HV kinematic single-track dynamics,

$$\Delta t_{\text{eff}} \leftarrow \text{clip}(\Delta t_{wc}, \Delta t_{\min}, \Delta t_{\max}), \quad (13)$$

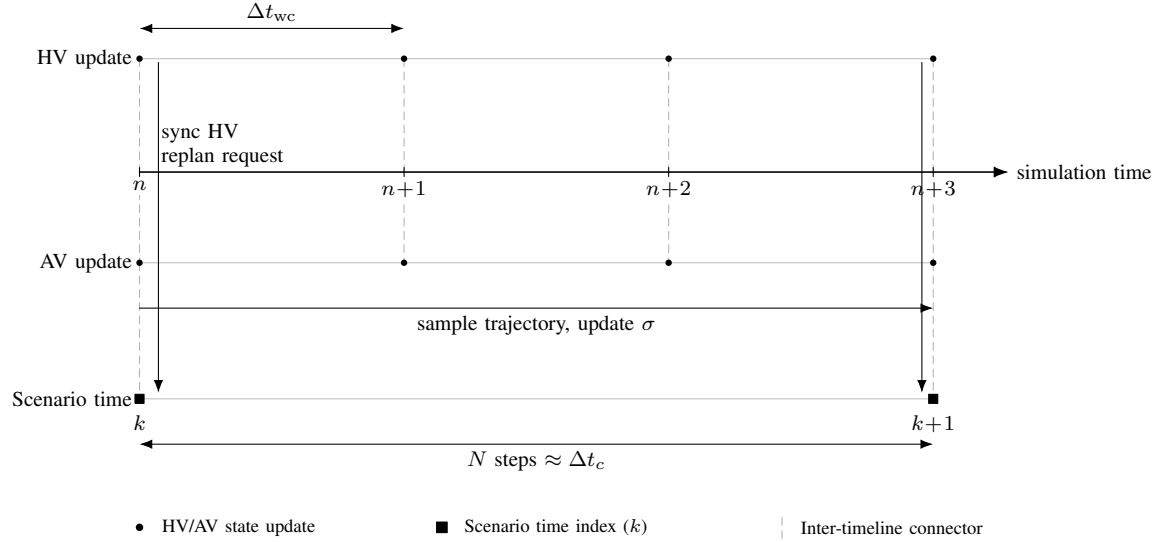


Fig. 4. Aligned HV/AV updates within the simulation loop. Each simulation step advances both vehicles by the measured wall-clock duration Δt_{wc} , while the scenario time index k advances every N steps (approximately one Δt_c), triggering obstacle synchronization and replanning. The example uses $N = 3$.

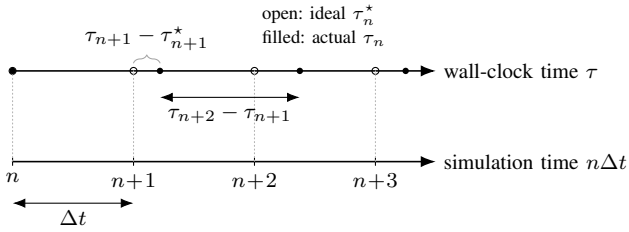


Fig. 5. Wall-clock and simulation time alignment. Open markers on the wall-clock axis indicate the *ideal* cycle-start schedule $\tau_n^* = t_0 + n\Delta t$, while the bottom axis advances uniformly in simulation steps $n\Delta t$. Filled markers indicate the *actual* wall-clock time τ_n at which each cycle begins; τ_n lags τ_n^* whenever the per-cycle computation exceeds the step budget Δt .

and the HV state is then propagated by $\Phi_{KS}(x_h, u_h, \Delta t_{\text{eff}})$ at the top of the next cycle (Algorithm 1, line 7; for brevity we write this argument as Δt_{wc} in Algorithm 1). The integrated HV motion thus reflects the actual elapsed real time while remaining numerically stable under transient overruns. The combination of wall-clock-anchored scheduling, drift-handling mechanisms, and measured-interval integration enforces the per-cycle invariant $\Delta t_{wc} \approx \Delta t$ under normal load.

b) Scenario-Time and Replanning Scheduler: Since the planner operates on its own time step Δt_c , a dedicated scheduler links the simulation time step Δt and the scenario time step Δt_c by computing an integer replanning period N in simulation steps and emitting a scenario time index k that advances every N simulation steps, thereby aligning the simulation step index n with the scenario time index k . Here, Δt is supplied by the global time-controller module, Δt_c is obtained from the scenario description, and the initial scenario time index k_0 is specified by the planning problem.

The replanning period is chosen as

$$N = \max\left(1, \text{round}\left(\frac{\Delta t_c}{\Delta t}\right)\right), \quad (14)$$

so that N simulation steps correspond approximately to one scenario time step. A scenario index k is initialized at k_0 and updated as follows:

- The simulation step index n increments by one every cycle.
- When n is a multiple of N , the system forms a new planning problem using the current AV (and human-obstacle) state at scenario time k and then increments $k \leftarrow k + 1$.

This ensures that, roughly every Δt_c seconds of simulated time, the scenario time index advances by one, and the planner is re-initialized at the correct scenario time.

c) Trajectory-Progress Tracker: Between replanning events, the AV executes the most recent planner trajectory while accounting for the different time discretizations used by the simulator and the planner. The planner trajectory τ is represented as a discrete sequence of states sampled on the scenario time grid with step size Δt_c . At each simulation step, the tracker maintains a continuous trajectory-progress variable σ , interpreted as a continuous index into this discrete sequence, and emits the planner state at progress σ to drive the AV update. The dynamics of σ within one simulation loop are visualized at the bottom of Fig. 4 by the arrow labeled “*sample trajectory, update σ* ”: at every simulation step on the AV row, σ is incremented and the trajectory is resampled, with σ traversing the scenario timeline between two consecutive scenario indices k and $k+1$.

The progress variable is advanced according to

$$\sigma \leftarrow \sigma + \frac{\Delta t}{\Delta t_c}, \quad (15)$$

so that a unit increase in σ corresponds to one scenario time step (Algorithm 1, line 14). The current AV state is then obtained by sampling the trajectory at the discrete index $\lfloor \sigma \rfloor$ and mapping the sampled state back to the simulation coordinate system via the inverse transform $T_{c \rightarrow s}$ (Algorithm 1, line 13).

When a new trajectory τ_{new} arrives from the planner, τ is replaced by τ_{new} and σ is realigned to the discrete state whose mapped simulation pose is closest to the current AV pose,

$$\sigma \leftarrow \arg \min_i \|T_{c \rightarrow s}(\tau[i]) - x_{\text{AV}}\|, \quad (16)$$

so as to avoid discontinuities in the executed motion (Algorithm 1, line 5).

B. Multi-threaded Simulation Architecture

We employ a simulation main loop that is intentionally decoupled from the computationally intensive replanning process by running replanning in a dedicated worker thread. The design has two objectives: (i) to maintain a main loop at a target update rate, and (ii) to update the state of AV whenever a new trajectory from the planner becomes available, without stalling the per-step simulation progression. Here, the *main loop* refers to the per-step simulation control loop running on the main thread (state updates, trajectory application, rendering, and logging), and the *target update rate* is the nominal step period Δt maintained by the wall-clock time controller.

1) *Decoupling the Replanning Workload from the Main Loop*: This section details how the decoupling is realized at the thread level. We first introduce the concurrency primitives that couple the main thread and the worker thread, then describe in turn the per-step pipeline executed on the main thread, the conditions under which a replanning request is issued, the worker-thread routine that produces a new trajectory, and the way each completed result is applied back to the main loop.

The simulation framework maintains the asynchronous replanning mechanism using a mutex and a condition variable along with a single-slot request/result buffer.

At each simulation step n , the main thread executes the following sequence:

- 1) **Update of the current AV trajectory.** If a newly computed planner trajectory is available from the worker thread, the shared *current-trajectory* buffer is updated; otherwise, the previously stored trajectory is retained.
- 2) **Propagation of the HV.** The current human control input is applied to the low-level vehicle model in the *simulation module* to advance the HV by one step and update its visualization pose. The corresponding CommonRoad [2] representation (dynamic obstacle in the scenario frame) is *not* updated at every step; it is refreshed only when a replanning request is assembled via obstacle synchronization.
- 3) **Advancement of the AV by trajectory tracking.** The AV state at this simulation step is obtained deterministically from the *currently stored* planner trajectory τ , which is a discrete sequence of states $\tau[0], \tau[1], \dots$ defined in the scenario frame, by retrieving the state at index

$\lfloor \sigma \rfloor$. The resulting state is then mapped back to the simulation frame via the inverse transform $T_{c \rightarrow s}$ and used to overwrite the AV pose and velocity for this step, *without* invoking the planner. This is the same operation as in Algorithm 1, line 13.

- 4) **Non-blocking periodic replanning trigger.** Every N simulation steps, a replanning request is formed and enqueued such that typically $N\Delta t \approx \Delta t_c$.

The full workflow is summarized in Algorithm 2, where the main thread runs at every simulation step (lines 1–10) and the worker thread runs independently (lines 11–17); the two threads cooperate through a single request slot `req`, a single result slot `res`, and a boolean busy flag `b` (`true` when the worker is processing a request), with N denoting the replanning interval in simulation steps and n the current simulation step index. The remainder of this paragraph walks through this workflow from the main thread’s perspective.

Triggering a new replan. At every simulation step, the main thread evaluates the joint condition $n \bmod N = 0 \wedge b = \text{false}$ before issuing a replan: the first conjunct enforces the scheduled interval and the second ensures the worker is idle (Algorithm 2, line 6). When both hold, the main thread packages a request containing the current AV state mapped to the scenario frame via $T_{s \rightarrow c}$ together with the synchronized HV obstacle, hands the request to the worker, and continues without waiting (Algorithm 2, lines 7–8). When either conjunct fails, the trigger is skipped, so the main loop never blocks on an in-progress planning task.

Worker execution. The worker thread blocks until a request arrives (Algorithm 2, line 12), runs the motion planner—a computation whose runtime may vary and substantially exceed Δt —and delivers the resulting trajectory back through the result slot before marking itself idle (Algorithm 2, lines 16–17). Because the planner runs on its own thread, its variable runtime does not constrain the per-step cadence of the main loop.

Applying a delivered result. At the start of every subsequent simulation step, the main thread first checks for a newly delivered trajectory; if one is present, it adopts the new trajectory and realigns the progress variable σ to the discrete state whose mapped simulation pose is closest to the current AV pose (Algorithm 2, lines 2–3; this realignment is the same operation as in Algorithm 1, line 5). Between issuing a request and receiving its result, the AV continues to track the most recent trajectory; when a fresher one arrives it is incorporated without any waiting, which is how the loop achieves full decoupling from the planner’s variable runtime.

C. HV Simulator Module

At each discrete control cycle with sampling time Δt , the HV simulator reads human driver inputs and converts them into control commands for a continuous-time kinematic single-track vehicle model. Two categories of input devices are supported: (i) continuous hardware devices, including a steering wheel and throttle/brake pedals, and (ii) discrete keyboard inputs. All input modalities are mapped to a unified

Algorithm 2 Asynchronous replanning workflow and shared request/result exchange between the main simulation loop and the replanning worker

Require: Replanning period N , step index n , shared request slot req , shared result slot res , busy flag b , mutex and condition variable

```

1: Main thread loop (executed at each simulation step)
2: if  $\text{res}$  is available then
3:   Apply trajectory; reset progress; clear  $\text{res}$ 
4: end if
5: Update HV state; retrieve AV state from the latest trajectory
6: if  $n \bmod N = 0$  and  $b = \text{false}$  then
7:   Package replanning inputs (AV state in scenario frame, synchronized obstacles)
8:   Write  $\text{req}$ ; set  $b \leftarrow \text{true}$ ; notify worker
9: end if
10: Advance to next step without waiting for replanning
11: Worker thread loop
12: Wait on condition until  $\text{req}$  is available or shutdown is requested
13: if shutdown is requested then
14:   Exit worker loop
15: end if
16: Copy  $\text{req}$ ; clear request slot
17: Run planner; write  $\text{res}$ ; set  $b \leftarrow \text{false}$ ; notify main thread

```

set of normalized control signals, which are subsequently processed by a common vehicle control abstraction.

1) Input Signal Processing:

a) Device Normalization: The framework supports two input devices—a steering-wheel-and-pedals rig (Logitech G923) and a keyboard—both of which are mapped to the same triplet $(p_{\text{th}}, p_{\text{br}}, s)$ used downstream by the vehicle-dynamics control. The hardware rig provides continuous measurements that are normalized linearly, whereas the keyboard provides only binary on/off signals that must be smoothed into continuous values by rate-limited integration.

Hardware. The steering wheel angle and pedal travel lengths are measured directly. Let $\ell_{\text{th}} \in [0, \ell_{\text{th}, \text{max}}]$ and $\ell_{\text{br}} \in [0, \ell_{\text{br}, \text{max}}]$ denote the physical throttle and brake pedal travel lengths, and let $\theta_{\text{sw}} \in [-\theta_{\text{sw}, \text{max}}, \theta_{\text{sw}, \text{max}}]$ denote the steering wheel angle relative to its mechanical limits. These raw measurements are linearly mapped to

$$\begin{aligned}
p_{\text{th}} &= \frac{\ell_{\text{th}}}{\ell_{\text{th}, \text{max}}} \in [0, 1], \\
p_{\text{br}} &= \frac{\ell_{\text{br}}}{\ell_{\text{br}, \text{max}}} \in [0, 1], \\
s &= \frac{\theta_{\text{sw}}}{\theta_{\text{sw}, \text{max}}} \in [-1, 1],
\end{aligned} \tag{17}$$

without further conditioning.

Keyboard. At each control cycle of period Δt , let $b_{\text{th}}, b_{\text{br}}, b_L, b_R \in \{0, 1\}$ denote the press states of the throttle (W/U_P), brake (S/Down/Space), left-steer (A/Left), and right-steer (D/Right) keys. Whenever both pedal keys are held simultaneously, braking takes precedence; we therefore define the effective throttle indicator $\beta_{\text{th}} \triangleq b_{\text{th}}(1 - b_{\text{br}})$, which equals 1 only when the throttle is held and the brake is not. Each pedal signal then ramps toward 1 at a key-specific rate while its (effective) key is active, and decays toward 0 at a

common release rate r_p^- otherwise:

$$\begin{aligned}
p_{\text{th}} &\leftarrow \text{clip}_{[0,1]}(p_{\text{th}} + [r_{\text{th}}^+ \beta_{\text{th}} - r_p^- (1 - \beta_{\text{th}})] \Delta t), \\
p_{\text{br}} &\leftarrow \text{clip}_{[0,1]}(p_{\text{br}} + [r_{\text{br}}^+ b_{\text{br}} - r_p^- (1 - b_{\text{br}})] \Delta t).
\end{aligned} \tag{18}$$

The steering signal accumulates toward $\pm s_{\text{max}}$ at rate r_s^+ while a steering key is held, and decays back to zero at rate r_s^- when neither is held:

$$s \leftarrow \begin{cases} \text{clip}_{[-s_{\text{max}}, s_{\text{max}}]}(s + r_s^+ (b_L - b_R) \Delta t), & b_L + b_R \geq 1, \\ \text{sgn}(s) \max(0, |s| - r_s^- \Delta t), & b_L = b_R = 0. \end{cases} \tag{19}$$

We use $r_{\text{th}}^+ = 1.8 \text{ s}^{-1}$, $r_{\text{br}}^+ = 2.5 \text{ s}^{-1}$, $r_p^- = 2.2 \text{ s}^{-1}$, $r_s^+ = 2.0 \text{ s}^{-1}$, $r_s^- = 3.5 \text{ s}^{-1}$, and $s_{\text{max}} = 0.65$; the steering cap is set below the full normalized range to keep the emulated wheel within a comfortable manual span. Small deadbands (10^{-3} for the pedals and 10^{-4} for the steering) are applied to suppress numerical noise.

The resulting triplet $(p_{\text{th}}, p_{\text{br}}, s)$ is consumed identically by the subsequent vehicle-dynamics control, regardless of which device produced it.

2) Vehicle Dynamics Control:

a) Longitudinal Control: The normalized throttle and brake pedal positions $p_{\text{th}}, p_{\text{br}} \in [0, 1]$ produced by Device Normalization are each mapped to a dimensionless *shaped pedal response* $\alpha \in [0, 1]$ through a smooth saturating function

$$\begin{aligned}
\alpha(p; k) &= 1 - e^{-kp}, \\
\alpha_{\text{th}} &= \alpha(p_{\text{th}}; k_{\text{th}}), \\
\alpha_{\text{br}} &= \alpha(p_{\text{br}}; k_{\text{br}}),
\end{aligned} \tag{20}$$

where the *shape parameter* $k > 0$ controls the steepness of the curve near the origin: a larger k produces a greater response at small pedal travel and saturates toward $\alpha = 1$ more quickly. Because $p \in [0, 1]$ and $k > 0$ imply $kp \geq 0$, the factor e^{-kp} lies in $(0, 1]$, so the response is bounded as $\alpha \in [0, 1]$ by construction—with $\alpha = 0$ at zero pedal travel and $\alpha = 1 - e^{-k}$ at full travel—and no explicit clamping is required. We use $k_{\text{th}} = 4$ for the throttle and $k_{\text{br}} = 3$ for the brake; the two curves are shown together with the linear identity $\alpha = p$ in Fig. 6.

The exponential form is adopted because (i) it is monotone, smooth, and differentiable on $[0, 1]$, which is convenient for downstream filtering and saturation; (ii) it yields finer-grained control at small pedal travel, the region in which drivers concentrate most of their pedal modulation [10], than the linear mapping $\alpha = p$; and (iii) it abstracts away detailed powertrain and brake-actuator transfer dynamics [11], which are not the focus of this work.

Given the current vehicle speed v , the maximum tractive force is constrained by both engine power and tire–road friction [11],

$$F_{\text{max}}(v) = \min\left(\frac{P_{\text{max}}}{|v| + \varepsilon_v}, \mu mg\right), \tag{21}$$

where P_{max} denotes the peak engine power, μ the tire–road friction coefficient, m the vehicle mass, g the gravitational

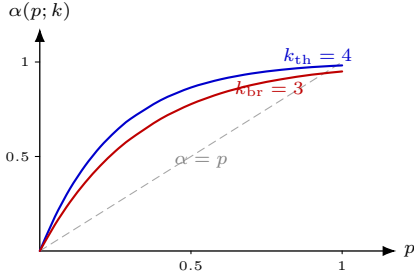


Fig. 6. Exponential pedal shaping $\alpha(p; k) = 1 - e^{-kp}$ used by the HV longitudinal controller, with the throttle gain $k_{th} = 4$ (blue) and the brake gain $k_{br} = 3$ (red); the linear identity $\alpha = p$ (dashed) is shown for comparison. A larger shape parameter k produces a steeper initial slope and earlier saturation toward $\alpha = 1$, which gives finer-grained control near rest while still approaching full drive/brake authority at larger pedal travel.

acceleration, and $\varepsilon_v > 0$ a small regularization constant preventing singularity at low speeds.

Resistive forces consist of aerodynamic drag and rolling resistance [12],

$$\begin{aligned} F_{\text{drag}} &= \frac{1}{2} \rho C_D A_f |v| v, \\ F_{\text{roll}} &= mg C_{rr} \text{sgn}(v), \end{aligned} \quad (22)$$

where ρ denotes air density, C_D the drag coefficient, A_f the frontal area, and C_{rr} the rolling resistance coefficient.

The resulting drive and brake forces are given by

$$\begin{aligned} F_{\text{drive}} &= \alpha_{th} F_{\text{max}}(v), \\ F_{\text{brake}} &= \alpha_{br} F_{\text{brake,max}}, \end{aligned} \quad (23)$$

where $F_{\text{brake,max}}$ denotes the maximum achievable braking force. The commanded longitudinal acceleration is then computed as

$$a_{\text{cmd}} = \text{sat}_{[-a_{\text{max}}, a_{\text{max}}]} \left(\frac{F_{\text{drive}} - F_{\text{brake}} - F_{\text{drag}} - F_{\text{roll}}}{m} \right), \quad (24)$$

where $a_{\text{max}} > 0$ denotes the maximum admissible longitudinal acceleration and $\text{sat}_{[a,b]}(\cdot)$ clamps its argument to the interval $[a, b]$.

To emulate drivetrain and brake dynamics, the commanded acceleration is filtered by a first-order lag with time constant $\tau_{\text{long}} > 0$,

$$\dot{a} = \frac{1}{\tau_{\text{long}}} (a_{\text{cmd}} - a) \iff a_{n+1} = a_n + \frac{\Delta t}{\tau_{\text{long}}} (a_{\text{cmd},n} - a_n), \quad (25)$$

where n denotes the discrete simulation step index and a is the filtered (delivered) longitudinal acceleration.

b) Lateral Control: The normalized steering input $s \in [-1, 1]$ is first mapped to a steering-wheel angle $\theta_{sw} = s \theta_{sw,\text{max}}$, where $\theta_{sw,\text{max}} = 7.85$ rad (450°). The corresponding *target front-wheel steering angle* δ^* is obtained by applying a variable steering ratio and enforcing physical limits. The target steering angle is computed as

$$\delta^* = \text{sat}_{[-\delta_{\text{max}}, \delta_{\text{max}}]} \left(\frac{\theta_{sw}}{R(v, \theta_{sw})} \right), \quad (26)$$

where $R(v, \theta_{sw})$ is a calibrated steering ratio obtained via lookup tables indexed by speed and steering angle, and $\delta_{\text{max}} = 0.91$ rad represents the physical front-wheel steering angle limit.

The steering-rate command supplied to the vehicle model is approximated by the discrete-time derivative of the steering angle,

$$\dot{\delta}_{\text{cmd}} = \frac{\delta^* - \delta}{\Delta t}, \quad (27)$$

where δ denotes the current front-wheel steering angle and Δt the simulation sampling time. This formulation is consistent with control interfaces commonly adopted in motion-planning benchmarks such as CommonRoad [2].

c) Trajectory Generation: The HV dynamics are driven by the steering-rate command $\dot{\delta}_{\text{cmd}}$ and the filtered longitudinal acceleration a , and are numerically integrated at each control cycle over the interval $[t, t + \Delta t]$. Repeating this procedure yields an HV trajectory consistent with the driver's inputs, while respecting physical limits (power and friction constraints, braking capacity, and steering bounds) and ensuring smoothness through input ramping and acceleration lag.

D. Drivability Detection Module

To monitor safety, the simulator optionally performs collision and road-compliance checks for the HV using the CommonRoad drivability-checker package [13]. Checks are evaluated at each control cycle using the current vehicle states only.

Let the HV simulator state at scenario time index k be $x_h^{\text{sim}} = [x_h, y_h, \delta_h, v_h, \psi_h]^\top$, consistent with the notation of the Low-Level Simulation Module. This state is mapped to a CommonRoad kinematic single-track (KS) state $x_h^k = (p_h^k, v_h^k, \psi_h^k, \delta_h^k)$ by applying the same sim-to-scenario rigid transform $T_{s \rightarrow c}$,

$$\begin{aligned} p_h^k &= R p_h^{\text{sim}} + \mathbf{d}, \\ \psi_h^k &= \text{wrap}_\pi(\psi_h^{\text{sim}} + \Delta\psi), \end{aligned} \quad (28)$$

where R , \mathbf{d} , and $\Delta\psi$ are the rotation, translation, and yaw offset of $T_{s \rightarrow c}$ defined by the Frame-Alignment Module. The index k corresponds to the nearest CommonRoad time step consistent with the simulator time and scenario sampling period.

a) Collision Detection: Each vehicle is approximated by a rectangle of length l and width w . The HV footprint is tested against a collision checker that aggregates static obstacles from the scenario and dynamic obstacles representing all ego vehicles at the same time step. A collision is declared if the checker reports an intersection between the HV and any obstacle.

b) Road-Compliance Detection: Road boundaries are converted into a collision object derived from the lanelet network. The HV is considered off-road if its rectangular footprint collides with this boundary object.

The drivability status is declared valid if neither collision nor off-road violation is detected; these checks can be enabled

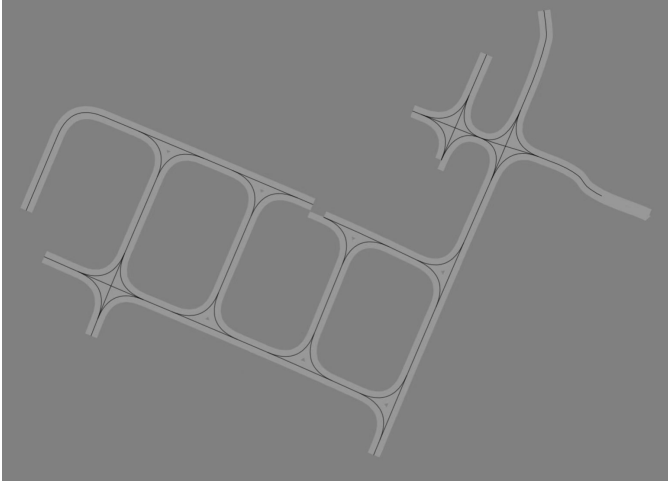


Fig. 7. Example road-network rendering in the visualisation module.

or disabled independently via configuration flags. Violations are reported in the simulator and can trigger a stop request for the HV to ensure safe termination.

E. Visualisation Module

The visualisation module renders the lanelet-based road network from the CommonRoad scenario, together with the current poses of the HV and the AV, into a live simulation window, providing the human driver with real-time visual feedback during the simulation. The road network is given by left and right lane boundaries represented as polylines in a global metric map frame. For visual rendering purposes, these geometric primitives are converted into filled lane surfaces and boundary curves within a fixed world window of size $W \times H$ (in meters). Fig. 7 shows an example road-network rendering.

F. Scenario Generation Module

This module converts runtime simulation data into standardized **CommonRoad scenario files**. It processes time-series state logs, including position, velocity, and orientation of all agents, and reconstructs the dynamic traffic environment in the CommonRoad XML format. By mapping the recorded trajectories of both AVs and HVs onto the underlying road network, the module generates high-fidelity replayable CommonRoad scenarios. These standardized outputs support offline verification, frame-by-frame visualization of interactions, and the sharing of representative interaction cases without requiring the original simulation environment.

IV. EVALUATION

This section provides a qualitative evaluation of the proposed simulation framework by replaying a recorded HV and analyzing the resulting interaction with an AV controlled by different planners. The simulator runs at a fixed time step of $\Delta t = 0.01$ s, while figures report representative state snapshots at coarser intervals for readability.

A. Single-AV Simulation with Different Planners

We consider a single-AV scenario in which an HV is actively controlled via keyboard input to exhibit aggressive interactive behaviors toward the AV. For each planning policy under evaluation, the HV applies a consistent set of challenging maneuvers, including sudden lane changes, intentional stopping in front of the AV, and deliberate obstruction of the AV’s intended path.

1) *The IDM Planner*: Fig. 8 shows per-frame state snapshots for the IDM planner². The sequence highlights a representative interaction in which the HV cuts in directly ahead of the AV and then stops; accordingly, the AV is driven to decelerate and come to a stop to maintain a safe gap. Fig. 9 provides a quantitative analysis of this interaction, displaying the heading angle, position, and velocity profiles of the AV.

2) *The Reactive Planner*: We next replace the IDM planner with a sampling-based reactive planner. Fig. 10 shows the corresponding per-frame simulation states. By leveraging a short-horizon prediction of the HV motion—assuming constant velocity and heading over the prediction interval—the reactive planner can proactively adjust its behavior, such as early deceleration or lane-change initiation, in response to the anticipated HV trajectory. As a result, the reactive planner executes a lane-change maneuver in this scenario, leading to closer and more dynamic AV–HV interaction. Fig. 11 further illustrates the quantitative performance of the reactive planner, showing the evolution of its heading, position, and velocity during the maneuver.

B. Multi-AV Simulation Capability

To demonstrate the scalability of the simulation framework, we further evaluate a multi-AV setup, where two AVs are simulated concurrently within the same CommonRoad [2] scenario. Each AV is controlled by an independent planner instance, while sharing a common simulation clock and road network representation. Fig. 12 presents a sequence of per-frame simulation states for a representative multi-AV scenario. The results show that the framework can consistently update and visualise the states of multiple vehicles without temporal inconsistencies, confirming its suitability for multi-agent simulation and evaluation. Fig. 13 provides a quantitative analysis of the multi-AV scenario, displaying the heading angle, position, and velocity profiles for the two AVs and the HV. The consistent and smooth evolution of these states for all agents further validates the framework’s capability to handle multi-agent dynamics and interactions effectively.

C. Timing Synchronization Performance

To evaluate the temporal fidelity of the mechanisms described in Section III-A2, we compare the proposed framework against a naive baseline that lacks explicit synchronization control. The experiment is conducted in a single-AV scenario using the IDM planner. Fig. 14 visualizes the cumulative ideal timeline and the realized wall-clock execution for both approaches, together with the evolution of step-wise and

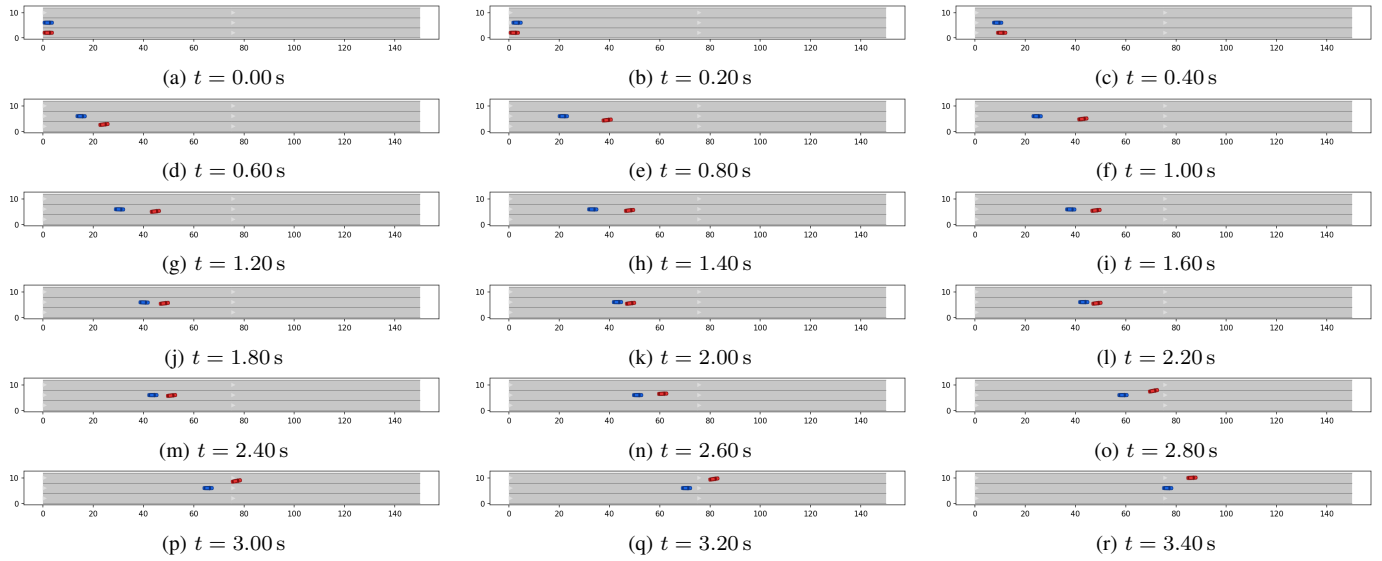


Fig. 8. IDM-planner per-frame state snapshots of the AV-HV interaction. The red car is the HV, and the blue car is the AV. Panels are shown at 0.2 s intervals (the simulator runs at $\Delta t = 0.01$ s). The sequence shows the HV cutting in directly ahead of the AV and coming to a stop, after which the AV decelerates and stops to maintain a safe gap.

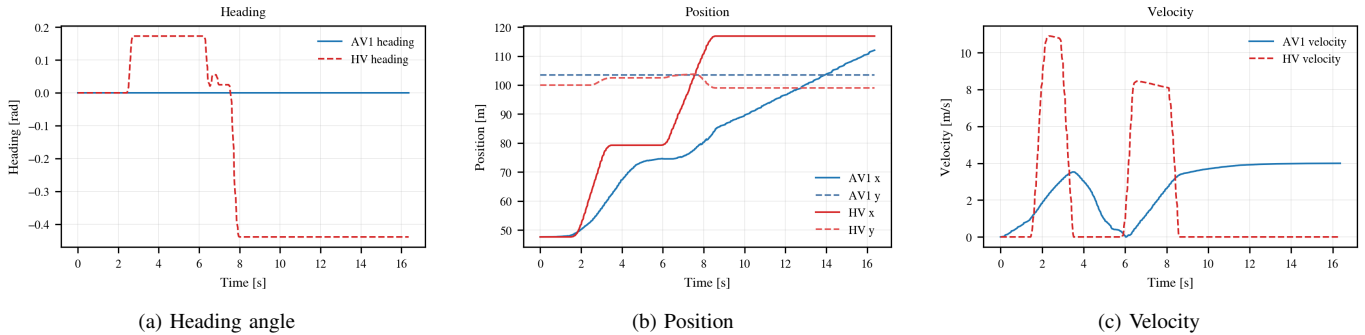


Fig. 9. Quantitative analysis of the IDM planner execution. (a) Heading angle profile, (b) Position trajectory, and (c) Velocity profile of the AV during the interaction.

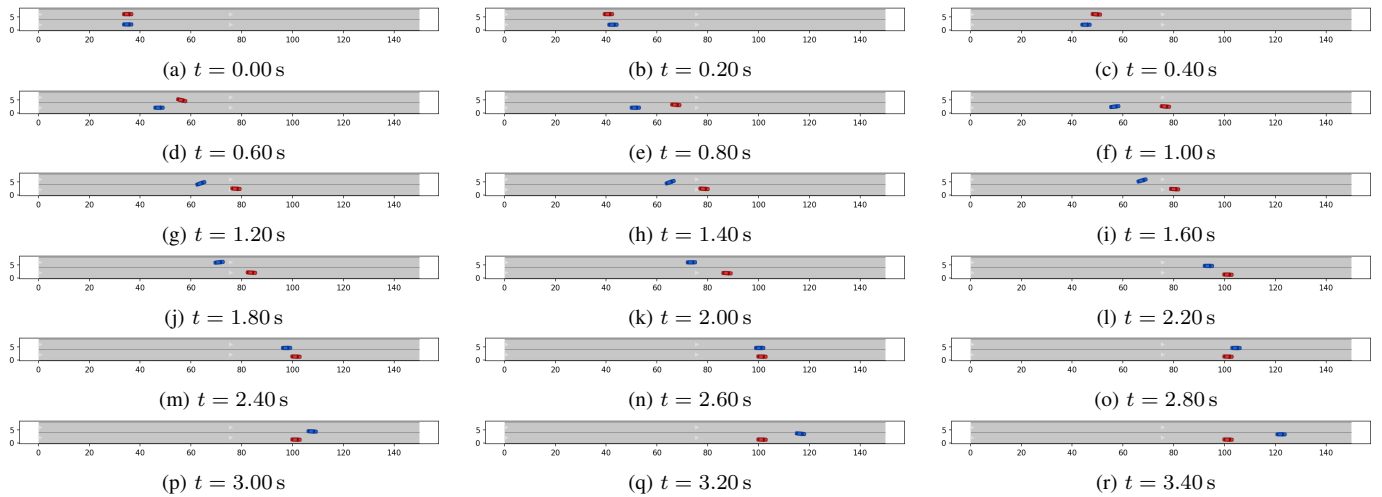


Fig. 10. Reactive-planner simulation state snapshots of the AV-HV interaction. The red car is the HV, and the blue car is the AV. Panels are shown at 0.2 s intervals (the simulator runs at $\Delta t = 0.01$ s). The sequence illustrates the AV executing a lane change while interacting with the HV.

accumulated timing errors. Table I summarizes the quantitative comparison. We define the timing behavior metrics as follows:

- **Final Error (E_f):** the absolute difference between sim-

ulation time and wall-clock time at the end of an experiment, indicating the residual drift after the synchronization mechanisms have acted.

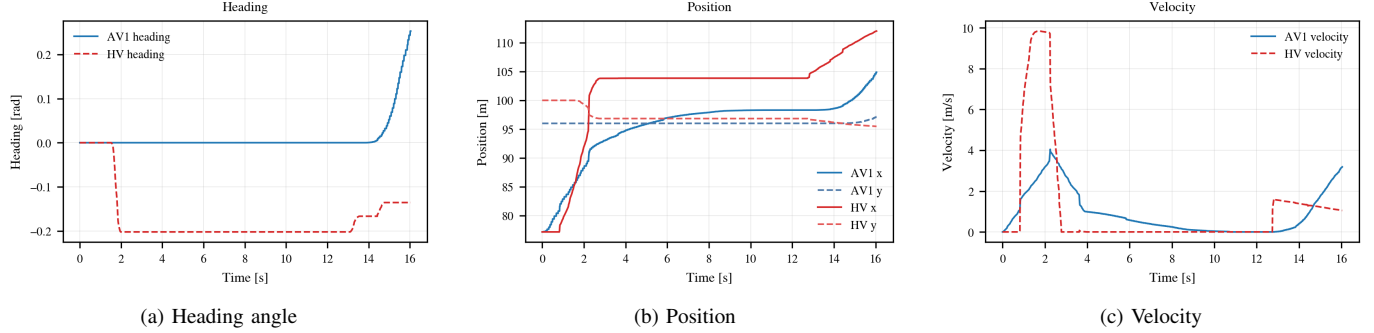


Fig. 11. Quantitative analysis of the Reactive planner execution. (a) Heading angle profile, (b) Position trajectory, and (c) Velocity profile of the AV during the interaction.

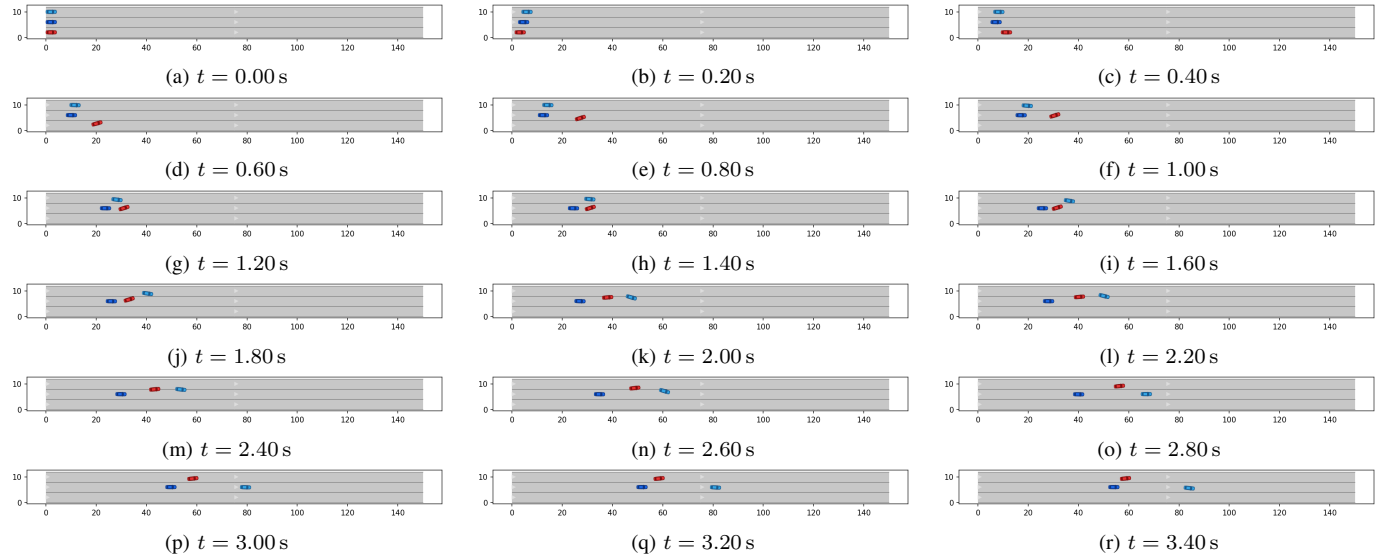


Fig. 12. Per-frame simulation states in a multi-AV scenario. The red car is the HV, and the blue cars are the AVs. Multiple AVs are simulated concurrently within the same road network. Panels are shown at 0.2 s intervals.

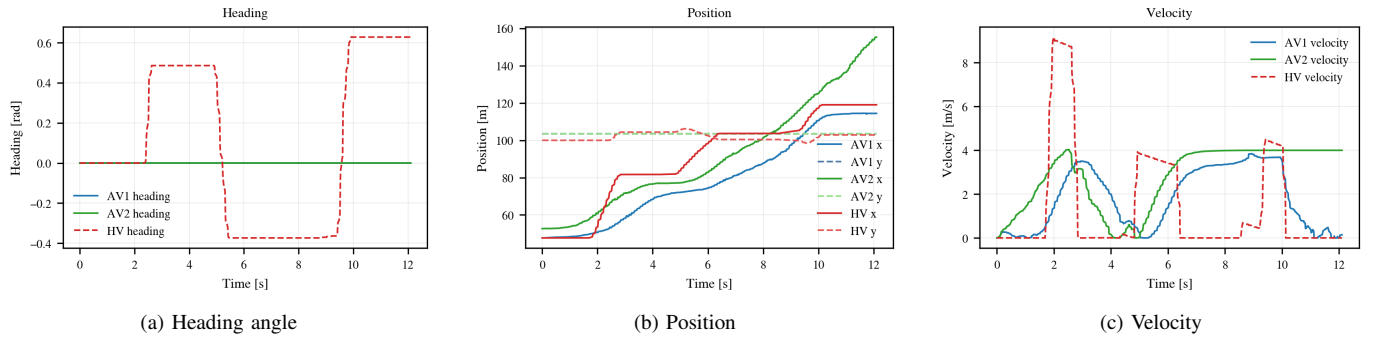


Fig. 13. Quantitative analysis of the Multi-AV scenario. (a) Heading angle profiles, (b) Position trajectories, and (c) Velocity profiles of the two AVs and the HV during the interaction.

- **Average Step Error** (\bar{e}_{step}): the mean absolute deviation of the realized step duration from the target step size (e.g., 10 ms), reflecting the stability of loop pacing.
- **Maximum Cumulative Error** (E_{max}): the maximum divergence between the ideal schedule and the realized execution over the full run, capturing the worst-case transient lag prior to recovery.
- **Timeout Ratio** (R_{timeout}): the fraction of simulation steps for which computation exceeds the available time

- budget (target step size). Larger values indicate sustained overload relative to real-time capacity.
- **Real-Time Ratio** (R_{RT}): the ratio between simulated time elapsed and wall-clock time elapsed. A value of 1.0 indicates perfect real-time execution. We report the average (\bar{R}_{RT}) and minimum ($R_{\text{RT,min}}$) values to characterize overall performance and worst-case slowdowns.
- **Time Efficiency** (η_t): the ratio of the total simulated duration to the total wall-clock duration of the experiment,

TABLE I
QUANTITATIVE COMPARISON OF TIMING SYNCHRONIZATION
PERFORMANCE

Metric	Proposed	Naive
<i>Time Performance</i>		
Final Error (E_f)	1.48 ms	402.38 ms
Average Step Error (\bar{e}_{step})	4.10 ms	22.84 ms
Maximum Cumulative Error (E_{max})	90.67 ms	1998.47 ms
Timeout Ratio ($R_{timeout}$)	37.7%	56.4%
<i>Real-time Performance</i>		
Final Real-Time Ratio (R_{RT})	1.00	0.97
Average Real-Time Ratio (\bar{R}_{RT})	0.99	0.84
Minimum Real-Time Ratio ($R_{RT,min}$)	0.10	0.04
<i>Efficiency</i>		
Time Efficiency (η_t)	99.99%	34.36%
Precision Ratio (P_r)	1.00×10^{-4}	2.85×10^{-2}

expressed as a percentage, providing a global measure of speed relative to real time.

- **Precision Ratio (P_r):** the ratio of the final timing error to the total wall-clock duration of the experiment, i.e., $P_r = E_f / (\tau_K - \tau_0)$, which normalizes residual drift by the overall experiment length.

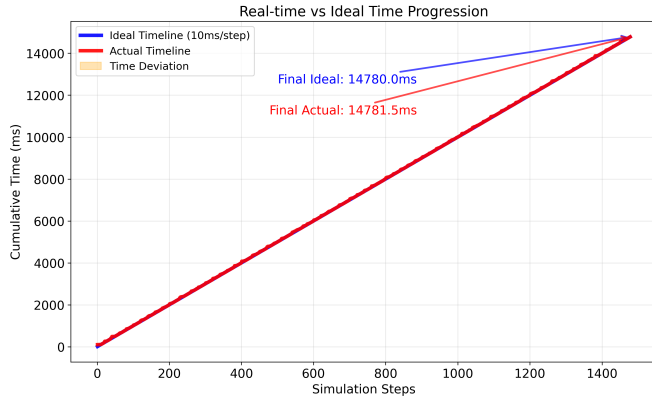
The results in Fig. 14 and Table I demonstrate the significant impact of the proposed synchronization mechanisms. While

the naive approach suffers from unbounded drift (reaching nearly 2000 ms) and poor time efficiency (34.36%), the proposed framework effectively bounds the maximum cumulative error (approx. 200 ms) and maintains near-perfect time efficiency (99.99%). This confirms that the explicit synchronization strategies—wall-clock pacing, drift reset, and adaptive frame skipping—are essential for maintaining temporal fidelity in real-time human-in-the-loop simulations.

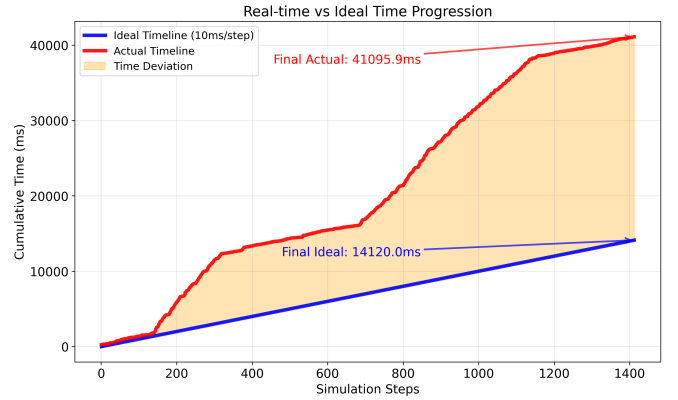
V. CONCLUSION

This paper presents CommonRoad-Game, a human-in-the-loop simulation framework tightly integrated with the CommonRoad ecosystem. Beyond serving as a testbed for autonomous driving motion planners, the framework enables systematic analysis of human driving behaviors and supports the generation of interactive traffic scenarios within a unified and reproducible setting.

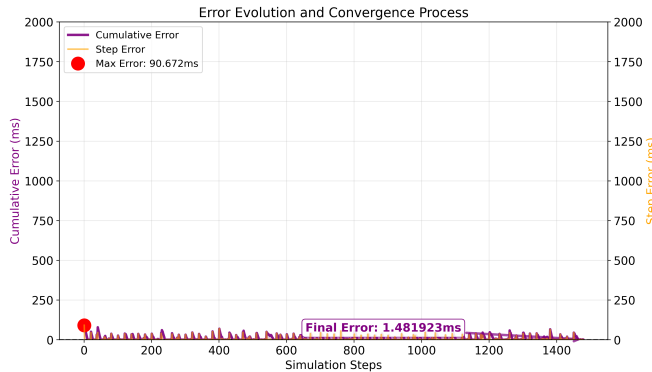
In contrast to existing simulation platforms, CommonRoad-Game is, to the best of our knowledge, the first framework to enable real-time human-in-the-loop interaction—through consumer input devices such as a keyboard or a steering-wheel-and-pedals interface—directly within standardized CommonRoad scenarios. This tight integration allows researchers to directly reuse standardized scenarios, maps, and evaluation pipelines, thereby bridging the gap between offline bench-



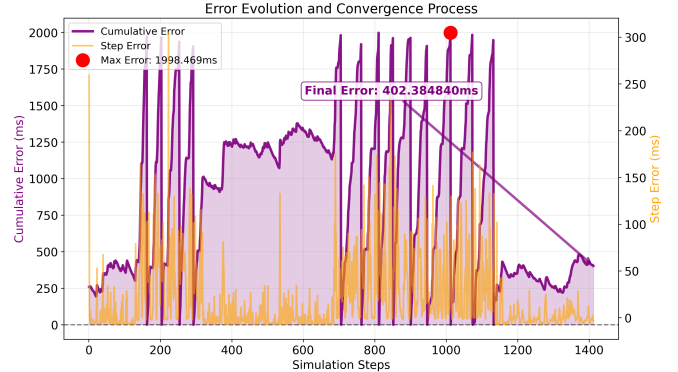
(a) Proposed: Timing Progression



(b) Naive: Timing Progression



(c) Proposed: Error Evolution



(d) Naive: Error Evolution

Fig. 14. Comparison of timing synchronization performance. Left column: Proposed framework with synchronization mechanisms. Right column: Naive baseline without explicit synchronization. (a, b) Cumulative timeline comparison. (c, d) Evolution of timing errors.

marking and interactive, human-in-the-loop experimentation.

Compared to mature, large-scale autonomous driving simulators, the proposed framework follows a lightweight design philosophy. By focusing on essential functionalities required for real-time interaction and behavioral studies, it reduces system complexity and computational overhead, making it more accessible for rapid prototyping and research-oriented use cases.

Furthermore, the framework explicitly addresses the often-overlooked discrepancy between simulation time and wall-clock time. Through a multi-threaded architecture with explicit synchronization mechanisms, CommonRoad-Game ensures temporal fidelity during real-time operation, preventing unbounded time drift and maintaining timing errors within a bounded range. This design choice is critical for experiments involving human participants, where consistent real-time responsiveness is required.

REFERENCES

- [1] W. Schwarting, A. Pierson, J. Alonso-Mora, S. Karaman, and D. Rus, "Social behavior for autonomous vehicles," *Proc. of the National Academy of Sciences*, vol. 116, no. 50, pp. 24 972–24 978, 2019.
- [2] M. Althoff, M. Koschi, and S. Manzingger, "CommonRoad: Composable benchmarks for motion planning on roads," in *Proc. of the IEEE Intelligent Vehicles Symposium*, 2017, pp. 719–726.
- [3] A. Dosovitskiy, G. Ros, F. Codevilla, A. Lopez, and V. Koltun, "CARLA: An open urban driving simulator," in *Proc. of the Conference on Robot Learning*, 2017, pp. 1–16.
- [4] G. Rong, B. H. Shin, H. Tabatabaee, Q. Lu, S. Lemke, M. Možeiko, E. Boise, G. Uhm, M. Gerow, S. Mehta *et al.*, "LGSVL simulator: A high fidelity simulator for autonomous driving," in *Proc. of the IEEE 23rd International Conference on Intelligent Transportation Systems*, 2020, pp. 1–6.
- [5] S. Shah, D. Dey, C. Lovett, and A. Kapoor, "AirSim: High-fidelity visual and physical simulation for autonomous vehicles," in *Field and Service Robotics*, 2018, pp. 621–635.
- [6] MAVLink Project, "MAVLink guide: Lightweight messaging protocol for drones," <https://mavlink.io/>, 2025, online.
- [7] Q. Li, Z. Peng, L. Feng, Q. Zhang, Z. Xue, and B. Zhou, "MetaDrive: Composing diverse driving scenarios for generalizable reinforcement learning," *IEEE Transactions on Pattern Analysis and Machine Intelligence*, vol. 45, no. 3, pp. 3461–3475, 2023.
- [8] Z. Cao, E. Biyik, W. Z. Wang, A. Raventos, A. Gaidon, G. Rosman, and D. Sadigh, "Reinforcement learning based control of imitative policies for near-accident driving," in *Proc. of Robotics: Science and Systems*, 2020.
- [9] G. Würsching and M. Althoff, "Robust and efficient curvilinear coordinate transformation with guaranteed map coverage for motion planning," in *Proc. of the IEEE Intelligent Vehicles Symposium*, 2024, pp. 2694–2701.
- [10] M. Treiber, A. Hennecke, and D. Helbing, "Congested traffic states in empirical observations and microscopic simulations," *Physical Review E*, vol. 62, no. 2, pp. 1805–1824, 2000.
- [11] R. Rajamani, *Vehicle Dynamics and Control*, 2nd ed. Boston, MA, USA: Springer, 2012.
- [12] T. D. Gillespie, *Fundamentals of Vehicle Dynamics*. Warrendale, PA, USA: Society of Automotive Engineers, 1992.
- [13] C. Pek, V. Rusinov, S. Manzingger, M. C. Üste, and M. Althoff, "CommonRoad drivability checker: Simplifying the development and validation of motion planning algorithms," in *Proc. of the IEEE Intelligent Vehicles Symposium*, 2020, pp. 1013–1020.